Article

Novel Application of Tagua Shell (*Phytelephas aequatorialis*) as Adsorbent Material for the Removal of Pb(II) Ions: Kinetics, Equilibrium, and Thermodynamics of the Process

Gino Alexander Chávez-Prado [1], Adams Brayan Benavides-García [1], Luis Angel Zambrano-Intriago [2,3], Naga Raju Maddela [2,4], Luis Santiago Quiroz-Fernández [5], Ricardo José Baquerizo-Crespo [1] and Joan Manuel Rodríguez-Díaz [1,3,*]

[1] Departamento de Procesos Químicos, Facultad de Ciencias Matemáticas, Físicas y Químicas, Universidad Técnica de Manabí, S/N, Avenida Urbina y Che Guevara, Portoviejo 130104, Ecuador; gchavez2734@utm.edu.ec (G.A.C.-P.); abenavides8215@utm.edu.ec (A.B.B.-G.); ricardo.baquerizo@utm.edu.ec (R.J.B.-C.)

[2] Instituto de Investigación, Universidad Técnica de Manabí, Portoviejo 130105, Ecuador; angel.zambrano@utm.edu.ec (L.A.Z.-I.); raju.maddela@utm.edu.ec (N.R.M.)

[3] Laboratorio de Análisis Químicos y Biotecnológicos, Instituto de Investigación, Universidad Técnica de Manabí, S/N, Avenida Urbina y Che Guevara, Portoviejo 130104, Ecuador

[4] Departamento de Ciencias Biológicas, Facultad de Ciencias de la Salud, Universidad Técnica de Manabí, Portoviejo 130105, Ecuador

[5] Instituto de Posgrado, Universidad Técnica de Manabí, S/N, Avenida Urbina y Che Guevara, Portoviejo 130104, Ecuador; santiago.quiroz@utm.edu.ec

* Correspondence: joan.rodriguez@utm.edu.ec

Abstract: Tagua shell is a material generated in the handcrafted jewelry industry, which is discarded since it does not have a specific use. The present study evaluates this material as an adsorbent for the removal of lead (II) in aqueous media. The adsorbent was characterized through the point of zero charge technique, X-ray microanalysis, scanning electron microscopy, and Fourier-transform infrared spectroscopy. Tests were carried out in a static system using a lead (II) solution of 100 mg·L^{-1} to establish the process conditions, setting a pH of 5, an adsorbent dose of 1.8 g/100 mL, and a contact time of 60 min. The kinetic study performed showed that the experimental data had a better fit with the pseudo-second order model. The experimental equilibrium data were correlated using the Langmuir, Freundlich, Toth, Redlich–Peterson, and Sips models, of which the Langmuir and Sips models proved to be the best to represent the adsorption process due to the high coefficient of determination they presented at the different temperatures, being between 0.9629–0.9899 and 0.9819–0.9900, respectively. The maximum amount of lead adsorbed was $22.0348 \text{ mg·g}^{-1}$ at a temperature of 298 K. Finally, the thermodynamics study indicated that the process is endothermic, spontaneous, and thermodynamically stable.

Keywords: adsorption; equilibrium; kinetics; lead; tagua shell; thermodynamics

1. Introduction

Water pollution is one of the most important environmental problems nowadays. This pollution has been caused by the increase in toxic substances coming mostly from untreated industrial effluent discharges. An example of this substance is lead (Pb), a heavy metal that, due to its nonbiodegradable nature, tends to accumulate in the ecosystem, generating an imbalance in the trophic chain and affecting human health [1]. According to the Environmental Protection Agency (EPA) and World Health Organization (WHO), the entry of Pb into the body either by ingestion, inhalation, or through the skin, can lead to serious problems, such as a lower intelligence quotient, hyperactivity, anemia, encephalopathy, miscarriages, cardiovascular problems, and decreased renal function [2–4].

The removal of lead and other heavy metals in water is performed by conventional methods, such as chemical precipitation, ion exchange, and reverse osmosis. These methods can be costly due to the technology used, and, in addition, they can generate other types of contaminants, such as sludge. Adsorption and especially the use of new adsorbents that do not require physical or chemical treatment for their use become a viable alternative for the treatment of heavy metals such as lead [1]. Adsorption is a separation process in which certain components present in a fluid are transferred to the surface of a porous solid material called an adsorbent [5]. When materials of biological origin are used as adsorbents, such as microorganisms (e.g., fungi and algae) and plant residue, it is known as biosorption [6]. A wide variety of materials of biological origin have been used to remove lead in aqueous solutions, for example, cocoa residues [7], *Eichhornia crassipes* [8], pineapple leaf fiber [9], and tomato waste and apple juice residue [10]. Tagua is a seed enveloped by a brown-colored coat. It comes from the *Phytelephas aequatorialis* palm commonly found in the west of Ecuador. The nanocellulose of this seed has been employed in the removal of heavy metals, such as cobalt, copper, and silver, being for the latter metal where a higher percentage of removal was achieved (>98%) [11]. However, there are no reports in the literature where tagua shell (TSH) has been used as an adsorbent for contaminants of any nature.

For this reason, the aim of the present study is the evaluation for the first time of TSH as an adsorbent material for the removal of Pb(II) in aqueous media. For this purpose, the adsorption mechanism is specifically analyzed through kinetic, equilibrium, and thermodynamic studies.

2. Materials and Methods

2.1. Adsorbent and Adsorbate

TSH was obtained in the community of Sosote, Manabí, Ecuador. TSH was triturated, sieved, and washed with abundant distilled water and dried in an oven (Memmert, Buechenbach, Germany) at 105 °C until a constant weight was obtained. $PbNO_3$ (obtained from Merk $\geq 99.5\%$) was used to prepare solutions of 20, 40, 60, 80, 100, 120, and 140 mg·L^{-1} of Pb(II). These solutions were prepared daily and stored at room temperature in amber glass vials. Concentrations were quantified using Inductively Coupled Plasma Optical Emission Spectroscopy (ICP-OES) instrument (Thermo Scientific ICap 6500 series inductively coupled plasma optical emission spectrometer) following the analytical standards detailed in "Standard Methods for the Analysis of Water and Wastewater" for Pb(II) detection [12]. All experiments were conducted in triplicate to ensure the reliability of the results.

2.2. Characterization

The point of zero charge (pHpzc) of TSH was determined by analyzing the variation in pH (2–11) of 25 mL of distilled water in contact with 0.1 g of adsorbent for 24 h at 300 rpm [13]. The pH was quantified using a Benchtop Fisher Scientific accumet AB150 pH meter. TSH surface morphology was determined through Scanning Electron Microscopy (SEM) and X-ray microanalysis (SEM/EDX) on a high resolution Scanning Electron Microscope (Schottky), with X-ray microanalysis and Electron Diffraction Pattern Analysis Retrodispersed: Quanta 400FEG ESEM/EDAX Genesis X4M. The specific surface area was calculated from the N_2 adsorption/desorption isotherms by using a surface area analyzer (Nova Station Quantachrome) and applying the Brunauer–Emmett–Teller (BET) equation [14]. The IR spectra of TSH before and after adsorption were performed in a NICOLET iS5 THERMO SCIENTIFIC Spectrometer, with a fast recovery deuterated triglycine sulfate detector (DTGS) and an optimized KBr/Ge medium infrared beam splitter. Spectra were obtained in the range of 4000 to 600 cm^{-1}.

2.3. Experimental Conditions of the Adsorption Process

The effect of the initial pH of the medium was studied using the HYDRA program developed by Ignasi Puigdomenech (2004) of the Division of Inorganic Chemistry, Royal Institute of Technology, Sweden. The diagrams were obtained with the lowest and highest concentration values of the metal species used. It is important to note that these diagrams were made considering only the properties of the aqueous solutions (concentration, pH, and ionic strength), without any consideration of the influence of the properties (shape, charge, mass, etc.) of the TSH used as adsorbent material.

The experimental adsorption tests were carried out in a static system, using an orbital shaker (New Brunswick Excella E24/E24R) with temperature control, in 250 mL flasks, with 100 mL of Pb(II) solution at 298 ± 1 K. All processed samples were filtered with Whatman quantitative filter paper (ashless, grade 589/3 blue ribbon). The adsorbent effect of the filter paper was analyzed, for which it showed nonsignificant differences < 1%. All tests were performed in triplicate with a variation of less than 5%. The adsorption capacity and the percentage of removal were obtained using Equations (1) and (2)

$$q_e = \frac{(C_o - C_e)V}{w} \tag{1}$$

$$\%R = \frac{(C_o - C_t)}{C_o} \times 100 \tag{2}$$

where q_e (mg·g^{-1}) is the adsorption capacity of the adsorbate-adsorbent system, C_o (mg·L^{-1}) is the initial adsorbate concentration, C_e (mg·L^{-1}) is the adsorbate concentration at equilibrium, V (mL) is the solution volume, and w (mg) is the mass of adsorbent. R is the percentage removal rate.

The adsorbent dose, effect of contact time, initial concentration, and temperature were evaluated in batch adsorption experiments. All experiments were performed by stirring 100 mL of Pb(II) solution at the required concentration with a dose of TSH in a 250 mL Erlenmeyer flask with stirring at a constant speed of 300 rpm. This shaking speed of 300 rpm was decided based on preliminary tests and published literature [15–17].

The effect of adsorbent dose (w) was studied by shaking a 100 mg·L^{-1} Pb(II) solution with different doses of TSH, ranging from 0.2 to 3.0 g per 300 min, at 298 K and pH 5.

The effect of contact time was performed with a solution of 100 mg·L^{-1} of Pb(II) applying the optimal w of TSH, 298 K, and pH 5, taking aliquots at times of 1, 3, 5, 10, 15, 20, 30, 40, 60, and 120 min.

The initial concentrations tested for the Pb(II) equilibrium study were in the range of 20 to 140 mg·L^{-1}, at a time of 60 min, 298 K, and pH 5.

2.4. Adsorption Kinetics and Equilibrium

The kinetic and equilibrium parameters were determined by employing nonlinear fitting methods using the Statistica 10.0 software.

The kinetic models of pseudo-first order, pseudo-second order, Elovich, Bangham, and Weber–Morris intraparticle diffusion were applied to interpret the kinetic data.

The pseudo-first order model is represented by the Lagergren equation (Equation (3)), where q_e and q_t are the amount of lead adsorbed at equilibrium and at time t (mg·g^{-1}), respectively, and k$_1$ (min^{-1}) is the adsorption rate constant [17].

$$log_{10}\left(\frac{q_e - q_t}{q_e}\right) = \frac{-k_1}{2.303}t \tag{3}$$

The pseudo-second order kinetic model is also based on the adsorption capacity of the solid phase and shows the behavior of the process along the contact time phase. It is

represented by Equation (4), where K_2 is the adsorption rate constant (g·mg^{-1}·min^{-1}), and q_e and q_t (mg·g^{-1}) are the amount of lead adsorbed at equilibrium and at time t (min) [17].

$$q_t = \frac{tK_2q_e^2}{1 + tK_2q_e} \tag{4}$$

The Bangham kinetic model can be used to verify if pore diffusion is the only rate-controlling step in the adsorption system employing this equation (Equation (5)), where K_B (mg·g^{-1}·s$^{-\alpha}$) and α_B (<1) are the empirical constants of the equation, and q_t (mg·g^{-1}) is the amount of adsorbate retained per unit adsorbent. If the experimental data can be represented by the equation, the adsorption kinetics can be limited by diffusion in the adsorbent pores [17,18].

$$q_t = K_B * t^{a_B} \tag{5}$$

For the Elovich model (Equation (6)), α (mg·g^{-1}·min^{-1}) and β (g·mg^{-1}) are Elovich constants obtained from the slope and the intercept of the linear plot of q_t vs. *Lnt*. This model assumes that the active sites of the bioadsorbent are heterogeneous and thus exhibit different activation energies, based on a second-order reaction mechanism [19].

$$q_t = \frac{1}{\beta} * Ln(\alpha * \beta) + \frac{1}{\beta} * Lnt \tag{6}$$

The Weber–Morris model is used to determine if the limiting step of the adsorption process occurs by intraparticle diffusion. Plotting the adsorption capacity of the adsorbent versus the square root of time, a straight line through the origin of the plane should be obtained. In Equation (7), K_{dif} (mg·g^{-1}·min$^{-0.5}$) is the Weber–Morris kinetic constant, and C is the constant related to the boundary layer. The authors have added this factor to provide an accurate representation of the possible difference in regression at the origin of the graph [17].

$$q_t = k_{dif}t^{0.5} + C \tag{7}$$

On the other hand, for the equilibrium study, the Langmuir, Freundlich, Toth, Redlich–Peterson, and Sips models were applied.

In the Langmuir model (Equation (8)), q_{max} (mg·g^{-1}) is the maximum amount of adsorbate per unit weight of adsorbent required to form a complete monolayer on the surface at high C_e, and K_L (L·mg^{-1}) is determined by graphing C_e/q_e vs. C_e [17].

$$q_e = \frac{K_L q_{max} C_e}{1 + K_L C_e} \tag{8}$$

With respect to the Freundlich model (Equation (9)), K_F and n are the constants (K_F is (mg·g^{-1}).(L·mg^{-1})$^{1/n}$, and n is dimensionless) [17].

$$q_e = K_F C_e^{1/n} \tag{9}$$

The Redlich–Peterson model, due to its versatility, allows the representation of an equilibrium adsorption system for a wide range of concentrations and can be applied for both homogeneous and heterogeneous adsorption processes. The nonlinear equation of this model is represented by Equation (10), where q_e (mg·g^{-1}) is the adsorption capacity at equilibrium, C_e (mg·L^{-1}) is the concentration of solute present in the solution at equilibrium; K_{RP} (L·g^{-1}), α_{RP} (L·mg^{-1}), and g are Redlich–Peterson parameters.

$$q_e = \frac{K_{RP}C_e}{1 + a_{RP}C_e^g} \tag{10}$$

The constant g ($0 \leq g \geq 1$) can characterize an isotherm. If g is close to 1, the isotherm is closer to the Langmuir isotherm, whereas if g is close to 0, the isotherm is closer to the Freundlich isotherm [20].

In the Toth model (Equation (11)), K_T (mg·g^{-1}) and α_T (L·mg^{-1}) are adsorption constants. z is a component that describes the degree of heterogeneity of the adsorption systems [20].

$$q_e = \frac{K_T * C_e}{[\alpha_T + C_e^z]^{\frac{1}{z}}}$$

(11)

In the Sips model (Equation (12)), q_{ms} (mg·g^{-1}) is the maximum amount of adsorbate adsorbed, C_e (mg·L^{-1}) is the concentration of the aqueous phase at equilibrium, and K_s (L·mg^{-1}) and n$_s$ are Sips constant [20].

$$q_e = \frac{q_{ms} K_s C_e^{n_s}}{1 + K_s C_e^{n_s}}$$

(12)

2.5. Adsorption Thermodynamics

The effect of temperature on the adsorption process was determined at temperatures of 288, 298, 308, and 318 K. The experiments were carried out using 100 mL of Pb(II) solution at different initial concentrations between 20 and 140 mg·L^{-1}, at pH 5, w appropriate, for 60 min at 300 rpm. The thermodynamic parameters, Gibbs free energy ($\Delta G°$) was calculated following Van 't Hoff equation (Equation (13)), where K_c is the constant obtained by multiplying the equilibrium constant by 55.5 and by 1000, and R is the gas constant (8.314 J·mol^{-1}·K^{-1}). The adsorption enthalpy ($\Delta H°$) and adsorption entropy ($\Delta S°$) were calculated by employing the adsorption data at different temperatures using Equation (14). The magnitude of $\Delta H°$ and $\Delta S°$ was calculated by the slope and the intersection of the *lnKc* vs. $1/T$ graph [17].

$$\Delta G° = -RT ln(K_c)$$

(13)

$$ln(K_c) = \frac{\Delta S}{R} - \frac{\Delta H}{RT}$$

(14)

3. Results and Discussion

3.1. TSH Characterization

The pHpzc has an important significance in adsorption processes, which indicates how the surface charge of the adsorbent is dependent on the pH of the solution. The pHpzc of TSH was measured by employing the pH drift method, as developed by Xie et al. [21]. Figure 1 shows the curves of the final pH of TSH vs. the initial pH and the initial pH (*x* axis) = final pH (*y* axis).
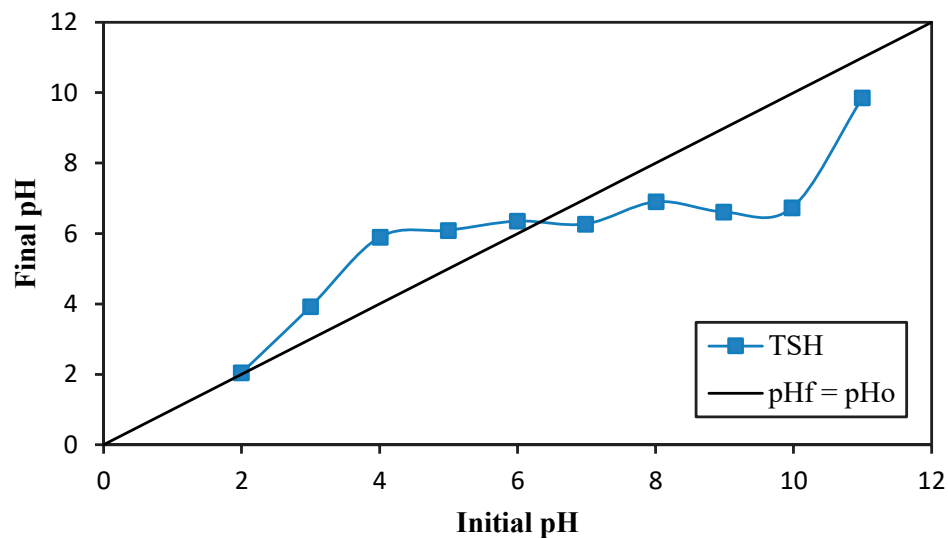

Figure 1. The point of zero charge (pH$_{pzc}$) of TSH.

The interception with the function $y = x$ is considered to be the pH_{pzc}, which is seven. In this context, the following can be explained:

1. The surface charge is positive when the pH of the solution is below seven, which favors anion adsorption;
2. The surface charge is negative when the solution pH is above seven, which favors cation adsorption, and;
3. The net charge of the adsorbents is zero when the pH is close to pH_{pzc}.

However, in this study, according to the effect of the solution pH on metal speciation (next section), the adsorption of Pb^{2+} cation as a function of pHpzc is not related. In this context, it is considered that other interactions may be stronger than the electrostatic forces alone so that the effect of surface charge is not so important. However, a cation often forms complexes with ligands, which are possibly negatively charged. In such a case, the cation is a negative complex, which can adsorb very well on a positively charged surface [22].

The adsorbent morphology was determined through the study of the micrograph (Figure 2a,e) obtained from SEM analysis. Irregular and rectangular fragments were observed, in the form of a skeletal structure, with the presence of linear fibers with pore-shaped holes. Positive energy spectrograms with X-ray microanalysis (EDX), obtained from SEM micrographs, show that TSH has regions with a high presence of C (darker fragments (Figure 2b; Z1)) and high proportions of Si and O (Figure 2c,d; Z2 and Z3). The high presence of Si in TSH is due to the high abundance of this mineral in the earth's crust, which is absorbed by plants and distributed mainly in the fruit peel. The C content is mainly due to the organic constitution of the plant with the presence of lignin, cellulose, and hemicellulose. In addition, the presence of various functional groups that have an affinity for metal complexation can be related, in many cases, in a nonselective manner, which favors Pb^{2+} adsorption. For this reason, the presence of Pb^{2+} on the adsorbent after adsorption was verified by EDX (Figure 2f; Z6). This behavior has been reported by different investigations using spectroscopic techniques that facilitate the complexation of metals [23].

The BET adsorption/desorption isotherms (Figure 3a) obtained by nitrogen physisorption showed a behavior corresponding to type IV, according to Brunauer's classification [24], typical of mesoporous materials. The high surface area determined, with a value of 100.58 $m^2 \cdot g^{-1}$, is due to the high content of organic matter present in TSH.

On the other hand, the FTIR spectra of TSH and TSH-Pb(II) are shown in Figure 3b. For this, the functional groups interacting in the adsorption were recognized. The FTIR revealed a band between 3000 and 3700 cm^{-1}, indicating the presence of hydrogen-bonded free OH groups and Si–OH groups on the surface of the adsorbent. After adsorption, this band showed a small stretching, related to the stretching of the OH band of the Si–OH group and the water adsorbed on the surface [25]. The peaks at 2920 and 2851 cm^{-1} were related to the stretching of the OH groups attached to methyl radicals. The peak at 2360 cm^{-1} was associated with the stretching of the –OH or C=O group of carboxylic acid. Then in TSH-Pb(II), this peak disappeared, showing the possible interaction of these groups with Pb(II). The peak at 1633 cm^{-1} in TSH confirmed the stretching of (–CO). However, it decreased at TSH-Pb(II), revealing the complex nature of the adsorption [26]. Finally, the stretching of the band at 1024 cm^{-1} could be assigned to the C–O of alcohols and carboxylic acids associated with the charge with the metal.

3.2. Effect of pH in Solution

Figure 4 shows the distribution diagram of lead in solution as a function of the pH for the concentration ranges studied ($20-140$ $mg \cdot L^{-1}$). It can be observed that for a pH lower than 6.1 the Pb^{2+} species remained constant. From pH 6.1 (lower concentration) and pH 5.7 (higher concentration), it can be observed that lead begins to precipitate forming $Pb(OH)_2$; this suggests that the process should be carried out at a pH lower than 5.7 to avoid the coexistence of two phenomena: adsorption and precipitation. This can be corroborated by

several other lead biosorption studies where results were obtained at a pH between 4 and 5.5 [27–29]. Based on the above, it was decided to use a pH of 5 for the following tests.
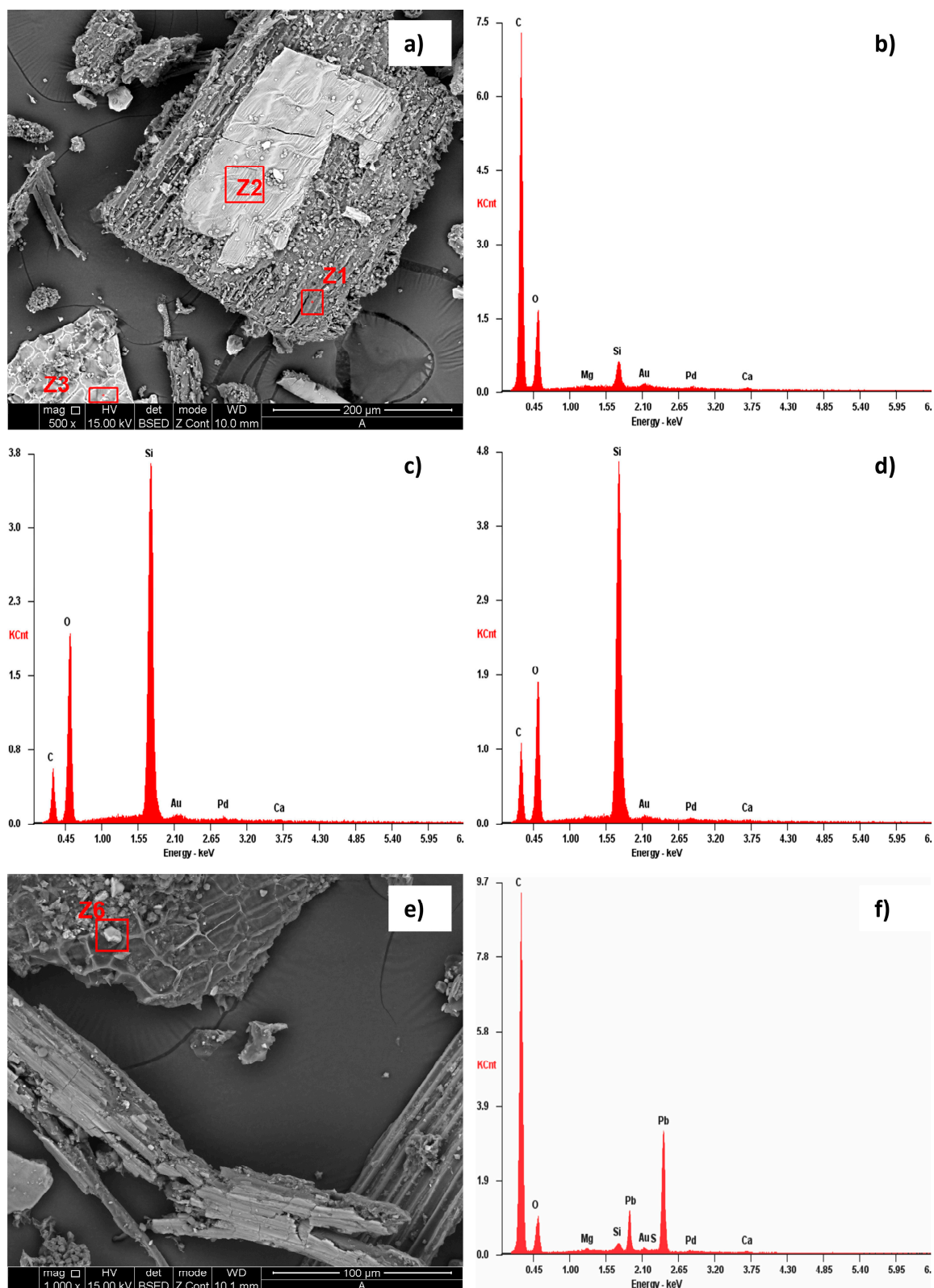
Figure 2. Scanning electron micrograph with SEM of TSH (**a**) and EDX spectrum of Z1 (**b**), Z2 (**c**), Z3 (**d**), Scanning electron micrograph with SEM of TSH/Pb(II) (**e**) and EDX spectrum of Z6 (**f**).

(**a**)

(**b**)
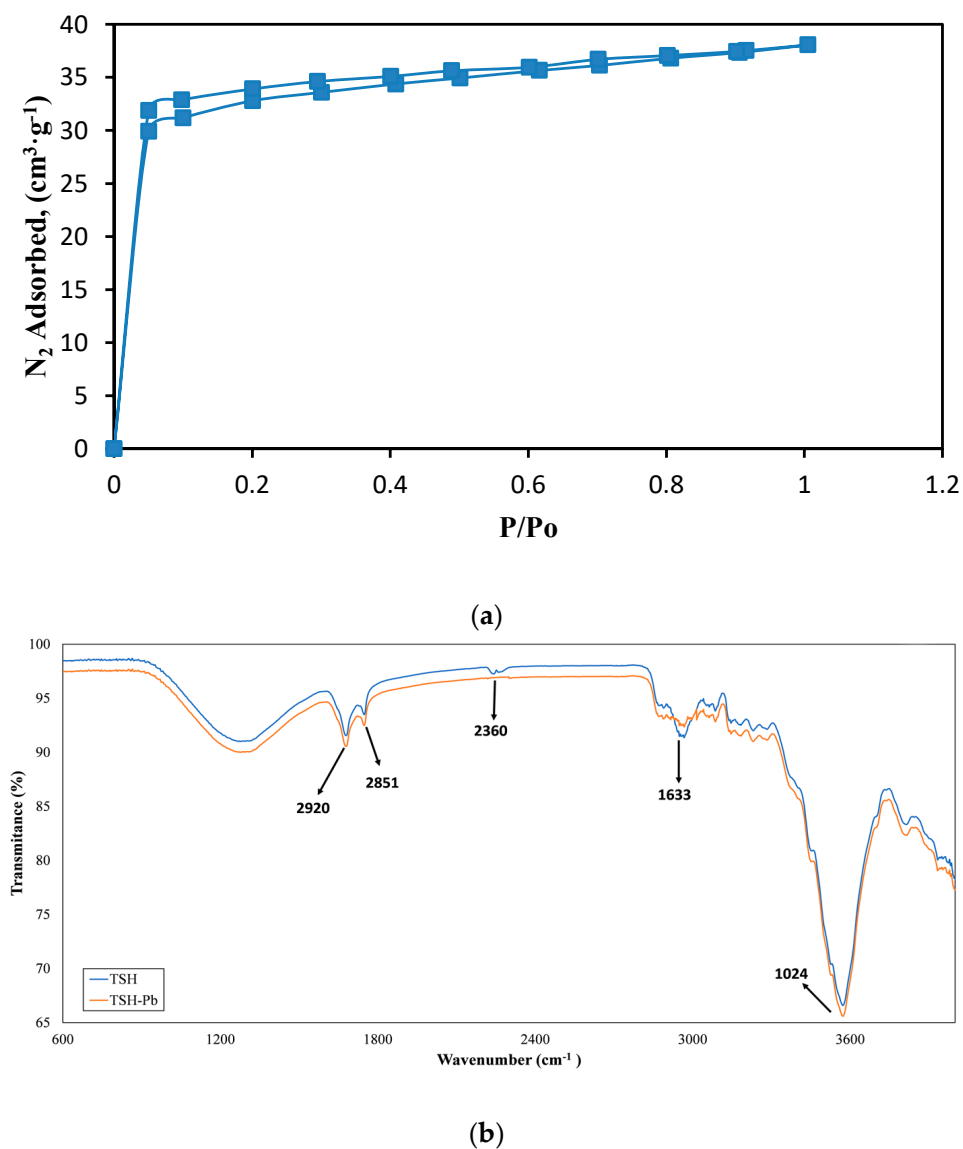
Figure 3. (**a**) Nitrogen adsorption and desorption isotherm at 77 K. (**b**) FT-IR spectrum for TSH and TSH-Pb(II).
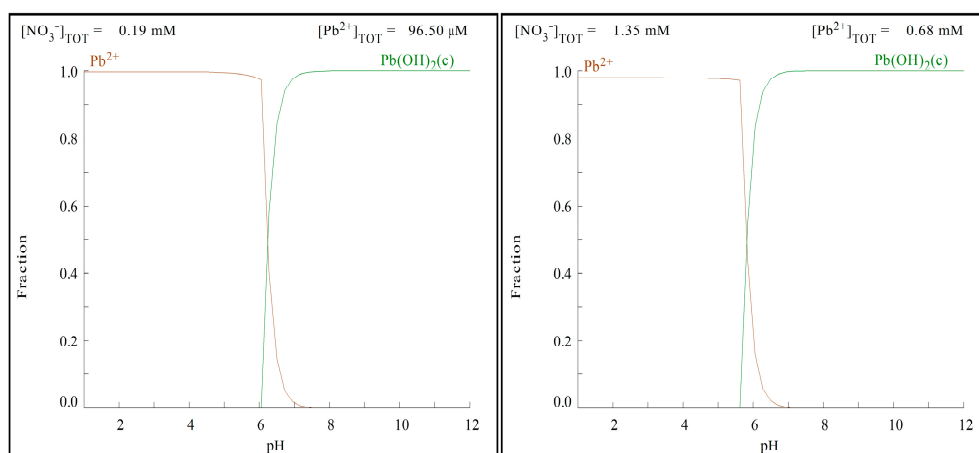
Figure 4. Distribution diagram of lead (II) complexes at various pHs.

3.3. Adsorbent Dose

Upon analyzing the adsorption capacity as a function of adsorbent dose (*w*) (Figure 5), in the range between 0.2 and 0.8 g/100 mL, there is a marked decrease in adsorption capacity, which subsequently remains constant. In numerical terms, 0.2 g/100 mL would indicate that this is the appropriate dose since it represents the highest adsorption capacity among the doses used. However, this represents an error of analysis due to the fact that Equation (1) contains *w* as the denominator, and when values < 1 are applied, the results will be higher [16]. This behavior can be corroborated by analyzing the *R*(%) curve, where it is clearly shown that the removal of Pb(II) is directly proportional to the increase in the dose used. Starting at 1.8 g of adsorbent, adsorbate removal did not vary significantly concerning higher amounts of biomass, which is why this amount was considered the appropriate dose for the following tests.
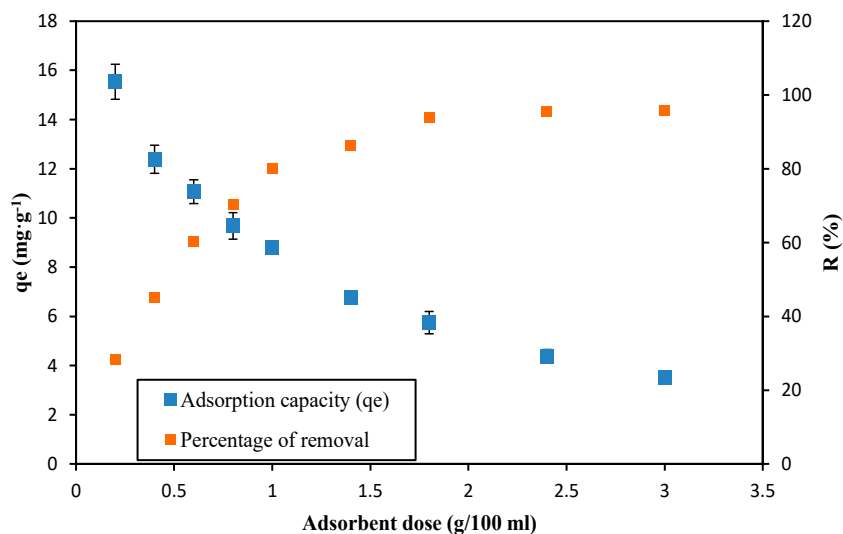
Figure 5. Effect of adsorbent dose on the removal of Pb(II) using TSH (*T* = 298 K, *t* = 300 min, and C_o = 100 mg·L^{-1}).

3.4. Contact Time

Figure 6 shows how lead removal increases as time passes. In the first 15 min of contact, adsorption occurred rapidly, removing about 90% of the lead. From this point on, the process occurred slowly until it reached equilibrium after 60 min, removing up to 96% of the metal.
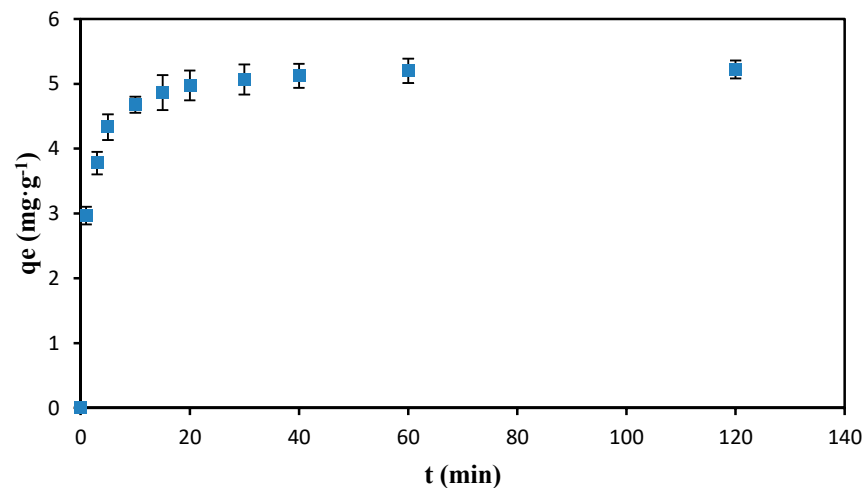
Figure 6. Effect of contact time on the removal of Pb(II) using TSH (*T* = 298 *K*, *t* = 120 min, C_o = 100 mg·L^{-1}, and pH = 5).

3.5. Adsorption Kinetics

The kinetic models used were the pseudo-first order, pseudo-second order, Elovich, Bangham, and intraparticle diffusion models. The parameters and fits of the kinetic models used are shown in Table 1 and Figure 7. The choice of the model that best fit the experimental data was made using the coefficient of determination (R^2) and the chi-square (X^2).

Table 1. Kinetic parameters of the pseudo-first order, pseudo-second order, Elovich, Bangham, and intraparticle diffusion models at a concentration of 20, 60, and 100 mg·L^{-1}.

Parameters	C_o (mg·L^{-1})		
	20	**60**	**100**
q_e,exp	0.9594 ± 0.0672	2.9022 ± 0.1265	5.2000 ± 0.1875
Pseudo-first order			
q_e,cal (mg·g^{-1})	0.9211	2.7081	4.9353
k_1 (min^{-1})	0.6333	0.6298	0.6743
R^2	0.6075	0.7088	0.7915
X^2	0.1136	0.2420	0.2775
Pseudo-second order			
q_e,cal (mg·g^{-1})	0.9687	2.8524	5.1885
k_2 (g·mg^{-1}·min^{-1})	1.1176	0.3687	0.2171
R^2	0.8620	0.9320	0.9736
X^2	0.0369	0.0547	0.0362
Elovich			
β (g·mg^{-1})	11.0310	3.6203	2.0958
α (mg·g^{-1}·min^{-1})	83.1308	179.1824	530.8156
R^2	0.8423	0.9164	0.8904
X^2	0.0333	0.0533	0.1223
Bangham			
K_B (mg·g^{-1}·s$^{-\alpha}$)	0.6491	1.8813	3.5107
α_B	0.1021	0.1066	0.0997
R^2	0.7982	0.8724	0.8402
X^2	0.0438	0.0848	0.1831
Intraparticle diffusion			
K_{dif1} (mg·g^{-1}·min$^{-0.5}$)	0.1198	0.4419	0.7950
C_1	0.4683	1.2320	2.3217
$R^2{}_1$	0.9681	0.9967	0.9351
K_{dif2} (mg·g^{-1}·min$^{-0.5}$)	0.0180	0.0528	0.1231
C_2	0.8832	2.4670	4.4025
$R^2{}_2$	0.6388	0.3060	0.9630
K_{dif3} (mg·g^{-1}·min$^{-0.5}$)	0.0095	0.0231	0.0189
C_3	0.8728	2.6754	5.0231
$R^2{}_3$	0.8020	0.6263	0.7359
X^2	0.0021	0.0051	0.0279

The pseudo-first order, Elovich, and Bangham models presented an R^2 value of 0.7915, 0.8904, and 0.8402 respectively, which were less than 0.9. Likewise, they presented a high X^2 value compared to the pseudo-second order model. Therefore, the pseudo-second order model was the best fit to the experimental data, presenting an R^2 of 0.9736. The fit to this model suggests that the removal mechanism is by chemisorption which implies the formation of chemical bonds between the adsorbate molecules and the adsorbent surface [30]. These results agree with studies conducted by Jeyakumar and Chandrasekaran [28] and Qaiser et al. [31], who used marine green algae and Ficus religiosa leaves, respectively, for the removal of lead ions and whose data were fit to the pseudo-second order model.
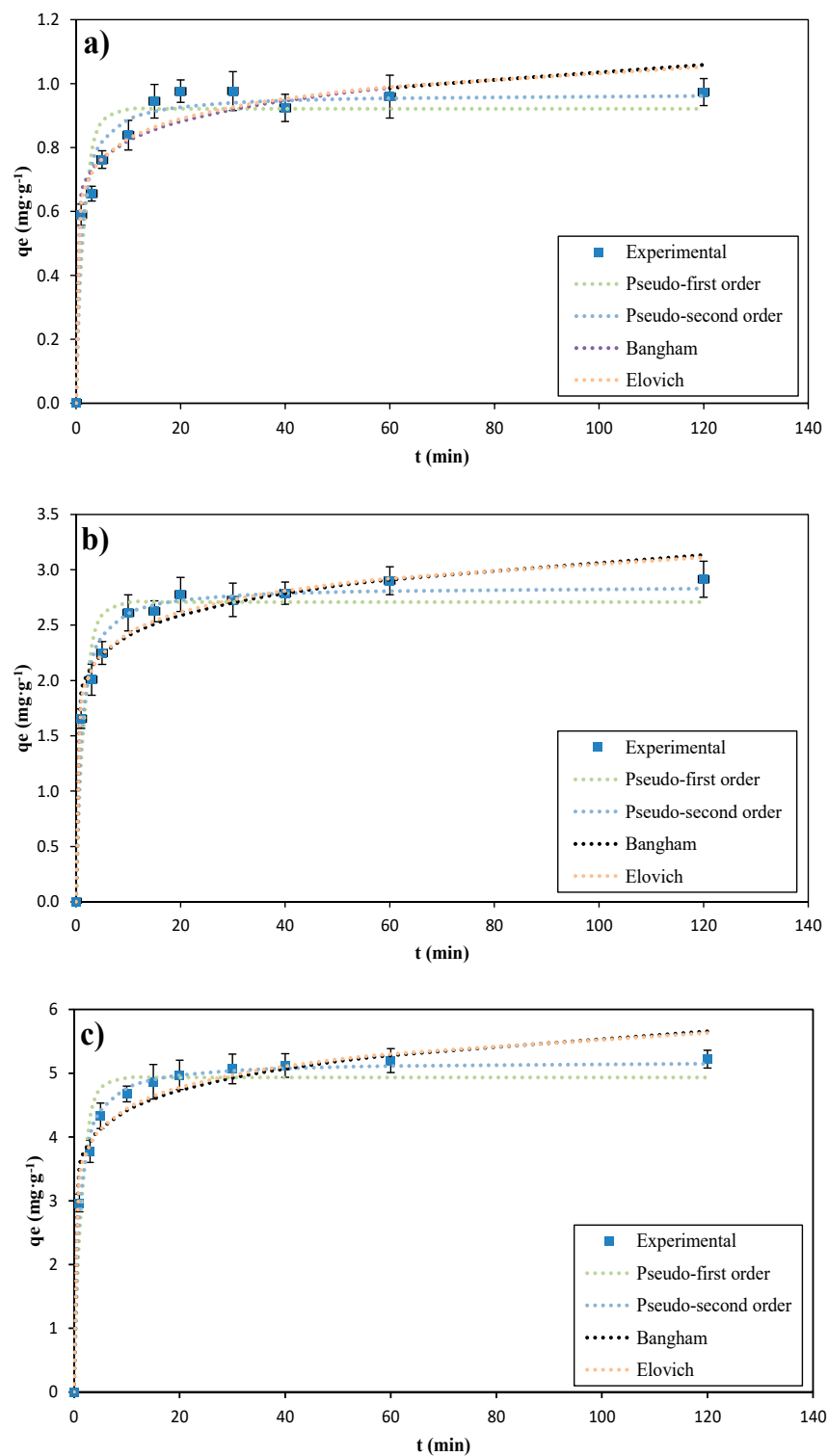
Figure 7. Pseudo-first order, pseudo-second order, Bangham, and Elovich kinetic models fitted to experimental data (w = 1.8 g and V = 100 mL) for different initial concentrations: (**a**) 20 mg·L^{-1}, (**b**) 60 mg·L^{-1}, and (**c**) 100 mg·L^{-1}.

To obtain a better interpretation of the adsorption mechanism of the process, the Weber–Morris intraparticle diffusion model was used. The graphical representation of this model (q_t vs. $t^{0.5}$) is given by three stages with a linear relationship and establishes that if any of these stages passes or is projected toward the origin of the graph, intraparticle diffusion will be the limiting stage of the process. However, if none of the stages meets this

condition or if there is multilinearity in the experimental data, the adsorption process can be controlled by several steps or a combination of them [17].

Figure 8 shows that all the stages behave in a linear way, and none passes through the origin, which means that intraparticle diffusion is not the limiting stage that controls the adsorption process. Despite this, this model allows us to describe the predominant mechanism by making an individual analysis for each stage. Through the values of the coefficients of determination R^2 and the diffusion constant K_{dif} of the first and second stages (Table 1), it can be indicated that the present adsorption process also has pore diffusion as a mechanism. Thus, there is a mass transfer or diffusion of Pb(II) from the solution to the adsorbent film and diffusion of Pb(II) over the pores of the adsorbent. On the other hand, the increase in C values from one stage to the other indicates that there is a greater effect on the boundary layer.
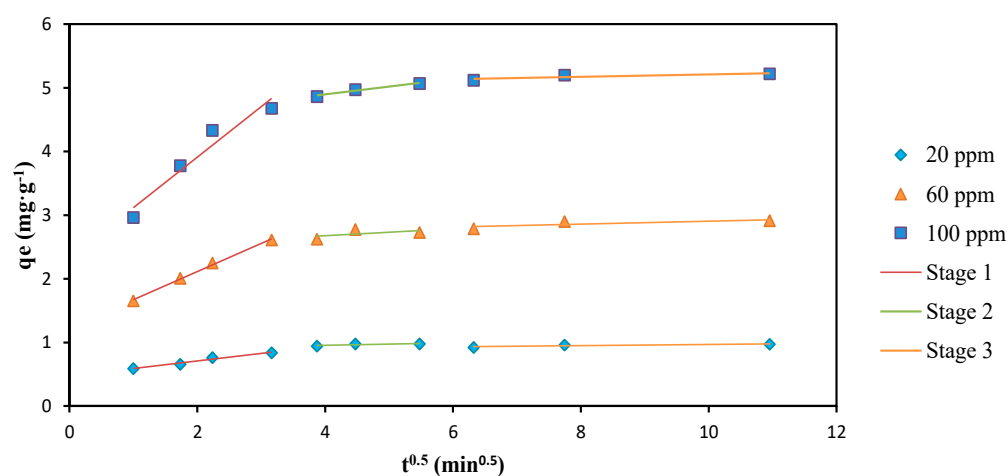
Figure 8. Weber–Morris intraparticle diffusion model fitted to experimental data with an initial concentration of 20, 60, and 100 mg·L^{-1} (T = 298 K, w = 1.8 g, V = 100 mL, and pH = 5).

3.6. Adsorption Isotherms

To optimize the design of the adsorption system, it is important to establish the most appropriate correlation. At this stage, the equilibrium study was carried out at different temperatures of 288, 298, 308, and 318 K. For their analysis, the Langmuir, Freundlich, Toth, Redlich–Peterson, and Sips models were applied, whose parameters and adjustments are shown in Table 2 and Figure 9. All models had a good fit to the experimental data at all temperatures studied; however, the best fit compared to the others were the Langmuir and Sips models with R^2 between 0.9629−0.9899 and 0.9819–0.9900, respectively. In this context, the Langmuir model indicates that in the adsorption process there is the formation of lead monolayers on the surface of the adsorbent and states that there are a finite number of identical and specific adsorption sites [32,33]. Its R$_L$ value was between 0 and 1 at all temperatures, indicating that the lead removal process has a favorable isothermal behavior. Also, it is shown that the maximum amount of adsorbed lead (q_{max}) was 22.0348 mg·g^{-1}.

On the other hand, the Sips isotherm is a model that combines the Langmuir and Freundlich expressions. It is used to predict heterogeneous adsorption systems and is very similar to the Langmuir isotherm with the difference that the Sips isotherm has a finite limit for very high concentrations. The way this model works is that at low adsorbate concentrations, it reduces to the Freundlich isotherm and at high concentrations, it reduces to the Langmuir isotherm, which predicts monolayer adsorption [17]. Therefore, based on the good fit obtained, it can be confirmed that monolayers are formed on the adsorbent surface when working with high concentrations, as established by the Langmuir model. In addition, this behavior corroborates that the mechanism of diffusion in the pores exists, according to the result of the Weber–Morris model.

Table 2. Parameters obtained from equilibrium models at different temperatures.

Isotherms	Parameters	Temperature (K)			
		288	298	308	318
Langmuir	q_e,exp	6.9468 ± 0.1838	7.0366 ± 0.3067	7.1277 ± 0.4989	6.7492 ± 0.3571
	q_{max}(mg·g^{-1})	21.5886	22.0348	18.2598	10.8976
	K_L(L·mg^{-1})	0.0372	0.0417	0.0577	0.0912
	R_L	0.57–0.16	0.55–0.15	0.46–0.11	0.35–0.07
	R^2	0.9629	0.9638	0.9843	0.9899
	X^2	0.3020	0.2988	0.1599	0.0767
Freundlich	KF [(mg·g^{-1})·(L·mg^{-1})$^{1/n}$]	0.8989	0.9997	1.1574	1.2587
	1/n	0.8087	0.8114	0.7651	0.5958
	R^2	0.9497	0.9509	0.9851	0.9779
	X^2	0.3949	0.3898	0.1960	0.2018
Toth	K_T (mg·g^{-1})	0.9024	18.7226	1.5253	1.8444
	α_T (L·mg^{-1})	−0.0511	22.8995	1.8839	1.8410
	1/z	0.1933	0.9628	0.3316	0.5241
	R^2	0.9496	0.9637	0.9860	0.9855
	X^2	0.4010	0.2260	0.1669	0.1161
Redlich–Peterson	K_{RP} (L·g^{-1})	3.8057	1.0153	2.2980	0.9100
	α_{RP} (L·mg^{-1})$^\beta$	3.2150	0.0986	1.0487	0.0525
	g	0.2391	0.7638	0.3625	1.1452
	R^2	0.9505	0.9603	0.9855	0.9900
	X^2	0.3976	0.3352	0.1832	0.0799
Sips	q_{ms} (mg·g^{-1})	8.9454	9.1036	13.0179	10.3128
	K_s (L·mg^{-1})	0.0316	0.0400	0.0734	0.0923
	n_s	1.8296	1.8175	11.515	1.0454
	R^2	0.9819	0.9823	0.9818	0.9900
	X^2	0.4221	0.4134	0.1604	0.0802
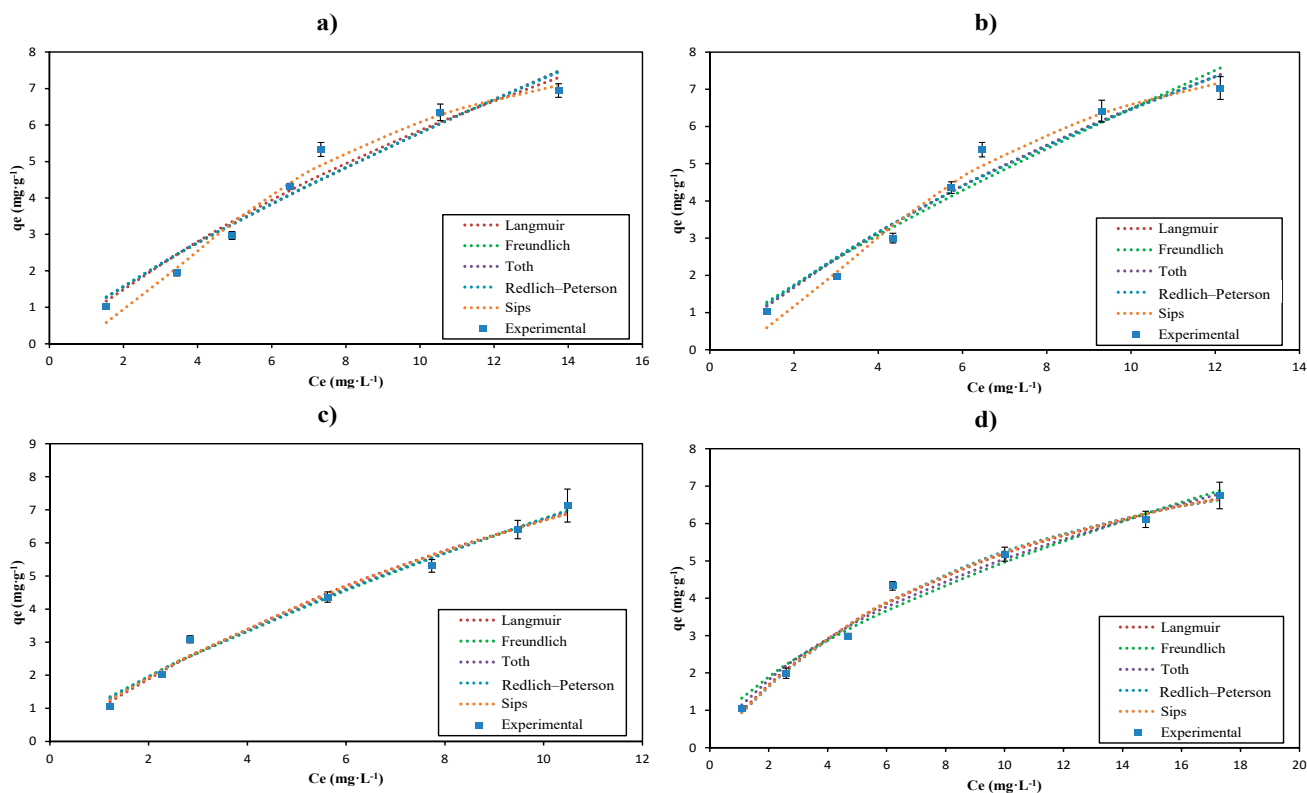
Figure 9. Langmuir, Freundlich, Toth, Redlich–Peterson and Sips adsorption isotherms: (**a**) 288 K, (**b**) 298 K, (**c**) 308 K, (**d**) 318 K. (w = 1.8 g, V = 100 mL, and t = 60 min).

3.7. Adsorption Thermodynamics

Thermodynamic parameters such as Gibbs free energy ($\Delta G°$), enthalpy ($\Delta H°$), and entropy ($\Delta S°$) obtained from Langmuir and Sips constants are shown in Table 3. The $\Delta G°$ was obtained from the Van 't Hoff equation, which also allowed us to obtain $\Delta H°$ and ΔS by graphing LnK vs. 1/T. It can be observed that the value of $\Delta G°$ decreases as the temperature increases, indicating that the lead adsorption process on TSH is spontaneous and thermodynamically stable. The positive value of $\Delta H°$ in both the Langmuir and Sips models indicates that the adsorption process is naturally endothermic. This result can be reaffirmed with the research conducted by Sekar et al. [34] and Ghahremani et al. [35], who used activated carbon prepared from coconut shell and nano Tricalcium phosphate, respectively, for the removal of lead ions from aqueous solutions and whose positive $\Delta H°$ values showed that the process exhibits an endothermic nature. Finally, the positive values of $\Delta S°$ indicate that there is an increase in randomness at the solute–liquid interface as the temperature increases. Furthermore, having positive $\Delta S°$ indicates that there is an increase in the degrees of freedom of the adsorbed species, and thus the high $\Delta S°$ indicates that there is a strong preference of Pb(II) for the adsorbent surface, suggesting the possibility of some structural change or rearrangement in the Pb(II)/TSH adsorption complex during the adsorption process.

Table 3. Thermodynamic parameters of the lead adsorption process.

Temperature (K)	$\Delta G°$ (KJ·mol^{-1})	$\Delta H°$ (KJ·mol^{-1})	$\Delta S°$ (J·K^{-1})
Langmuir			
288	-18.0468	22.7687	141.7204
298	-19.4640		
308	-20.8812		
318	-22.2984		
Sips			
288	-17.6957	26.2589	152.6201
298	-19.2219		
308	-20.7481		
318	-22.2743		

4. Conclusions

The results demonstrate that TSH, a byproduct of the handcrafted jewelry industry, can be used as an economical, selective, and efficient adsorbent for the treatment of wastewater contaminated with Pb(II). Residual TSH used in the present study was efficient for the adsorption of Pb(II) in aqueous media; using a minimum amount of adsorbent, it achieved a removal rate close to 96% in 60 min. The good fit of the experimental data with the pseudo-second order model and the multilinearity in the intraparticle diffusion of the Weber–Morris model, indicated that the predominant mechanisms of the system were chemisorption and film and pore diffusion, respectively. Through the equilibrium study, it was determined that the Langmuir and Sips isotherms had the best fits to the experimental data, indicating that in the adsorption process, adsorbate–adsorbent monolayer formation occurs. In this context, as a result of the good fit of the Langmuir and Sips isotherms, the thermodynamic equilibrium of the system was described with good accuracy, representing positive enthalpies that demonstrate that the process is endothermic, spontaneous, and thermodynamically stable.

Author Contributions: Writing—original draft preparation, G.A.C.-P. and A.B.B.-G.; writing—review and editing, L.A.Z.-I., N.R.M., L.S.Q.-F., R.J.B.-C. and J.M.R.-D. All authors have read and agreed to the published version of the manuscript.

Institutional Review Board Statement: Not applicable.

Informed Consent Statement: Not applicable.

Data Availability Statement: The data presented in this study are available on request from the corresponding author.

Conflicts of Interest: The authors declare no conflict of interest.

References

1. Barakat, M.A. New trends in removing heavy metals from industrial wastewater. *Arab. J. Chem.* **2011**, *4*, 361–377. [CrossRef]
2. EPA. Learn about Lead. Available online: https://www.epa.gov/lead/learn-about-lead (accessed on 3 November 2021).
3. Wani, A.L.; Ara, A.; Usmani, J.A. Lead toxicity: A review. *Interdiscip. Toxicol.* **2015**, *8*, 55–64. [CrossRef] [PubMed]
4. WHO. Lead Poisoning and Health. Available online: https://www.who.int/news-room/fact-sheets/detail/lead-poisoning-and-health (accessed on 3 November 2021).
5. McCabe, W.L.; Smith, J.C.; Harriott, P. *Unit Operations of Chemical Engineering*, 5th ed.; McGraw-Hill: Singapore, 1993.
6. Shamim, S. Biosorption of Heavy Metals. *Biosorption* **2018**, *2*, 21–49. [CrossRef]
7. Tejada-Tovar, C.; Lopez-Cantillo, K.; Vidales-Hernandez, K.; Villabona-Ortíz, A.; Acevedo-Correa, D. Kinetics and bioadsortion equilibrium of lead and cadmium in batch systems with cocoa shell (*Theobroma Cacao* L.). *Contemp. Eng. Sci.* **2018**, *11*, 1111–1120. [CrossRef]
8. Shekinah, P.; Kadirvelu, K.; Kanmani, P.; Senthilkumar, P.; Subburam, V. Adsorption of lead(II) from aqueous solution by activated carbon prepared from Eichhornia. *J. Chem. Technol. Biotechnol.* **2002**, *77*, 458–464. [CrossRef]
9. Daochalermwong, A.; Chanka, N.; Songsrirote, K.; Dittanet, P.; Niamnuy, C.; Seubsai, A. Removal of Heavy Metal Ions Using Modified Celluloses Prepared from Pineapple Leaf Fiber. *ACS Omega* **2020**, *5*, 5285–5296. [CrossRef]
10. Heraldy, E.; Lestari, W.W.; Permatasari, D.; Arimurti, D.D. Biosorbent from tomato waste and apple juice residue for lead removal. *J. Environ. Chem. Eng.* **2018**, *6*, 1201–1208. [CrossRef]
11. Noboa Zaldumbide, M.A. *Nanocelulosa de Tagua Como Agente Para Captación y Recuperación de Metales Pesados y Preciosos en Cuerpos de Agua*; Pontificia Universidad Católica del Ecuador: Quito, Ecuador, 2017.
12. Baird, R.B.; Eaton Andrew, D.; Rice Eugene, W. *Standard Methods for the Examination of Water and Wastewater*, 23rd ed.; American Public Health Association: Washington, DC, USA, 2017.
13. Campos, N.F.; Barbosa, C.M.B.M.; Rodríguez-Díaz, J.M.; Duarte, M.M.M.B. Removal of naphthenic acids using activated charcoal: Kinetic and equilibrium studies. *Adsorpt. Sci. Technol.* **2018**, *36*, 1405–1421. [CrossRef]
14. Rodríguez-Díaz, J.M.; García, J.O.P.; Sánchez, L.R.B.; da Silva, M.G.C.; da Silva, V.L.; Arteaga-Pérez, L.E. Comprehensive Characterization of Sugarcane Bagasse Ash for Its Use as an Adsorbent. *BioEnergy Res.* **2015**, *8*, 1885–1895. [CrossRef]
15. Jaerger, S.; dos Santos, A.; Fernandes, A.N.; Almeida, C.A.P. Removal of p-Nitrophenol from Aqueous Solution Using Brazilian Peat: Kinetic and Thermodynamic Studies. *Water Air Soil Pollut.* **2015**, *226*, 236. [CrossRef]
16. Andrade, C.A.; Zambrano-Intriago, L.A.; Oliveira, N.S.; Vieira, J.S.; Quiroz-Fernández, L.S.; Rodríguez-Díaz, J.M. Adsorption Behavior and Mechanism of Oxytetracycline on Rice Husk Ash: Kinetics, Equilibrium, and Thermodynamics of the Process. *Water Air Soil Pollut.* **2020**, *231*, 103. [CrossRef]
17. Zambrano-Intriago, L.A.; Gorozabel-Mendoza, M.L.; Córdova Mosquera, A.; Delgado-Demera, M.H.; Duarte, M.M.M.B.; Rodríguez-Díaz, J.M. Kinetics, equilibrium, and thermodynamics of the blue 19 dye adsorption process using residual biomass attained from rice cultivation. *Biomass Convers. Biorefinery* **2020**. [CrossRef]
18. Nguyen, D.T.C.; Le, H.T.N.; Do, T.S.; Pham, V.T.; Lam Tran, D.; Ho, V.T.T.; Tran, T.V.; Nguyen, D.C.; Nguyen, T.D.; Bach, L.G.; et al. Metal-Organic Framework MIL-53(Fe) as an Adsorbent for Ibuprofen Drug Removal from Aqueous Solutions: Response Surface Modeling and Optimization. *J. Chem.* **2019**, *2019*, 5602957. [CrossRef]
19. Tovar, C.; Herrera, A.; Ruiz, E. Kinetic and isotherms of biosorption of Hg(II) using citric acid treated residual materials. *Ing. Y Compet.* **2016**, *18*, 117–127. [CrossRef]
20. Wang, J.; Guo, X. Adsorption isotherm models: Classification, physical meaning, application and solving method. *Chemosphere* **2020**, *258*, 127279. [CrossRef] [PubMed]
21. Xie, A.; Dai, J.; Chen, X.; He, J.; Chang, Z.; Yan, Y.; Li, C. Hierarchical porous carbon materials derived from a waste paper towel with ultrafast and ultrahigh performance for adsorption of tetracycline. *RSC Adv.* **2016**, *6*, 72985–72998. [CrossRef]
22. Ambaye, T.G.; Vaccari, M.; van Hullebusch, E.D.; Amrane, A.; Rtimi, S. Mechanisms and adsorption capacities of biochar for the removal of organic and inorganic pollutants from industrial wastewater. *Int. J. Environ. Sci. Technol.* **2021**, *18*, 3273–3294. [CrossRef]
23. Sud, D.; Mahajan, G.; Kaur, M.P. Agricultural waste material as potential adsorbent for sequestering heavy metal ions from aqueous solutions—A review. *Bioresour. Technol.* **2008**, *99*, 6017–6027. [CrossRef]
24. Brunauer, S.; Emmett, P.H.; Teller, E. Adsorption of Gases in Multimolecular Layers. *J. Am. Chem. Soc.* **1938**, *60*, 309–319. [CrossRef]

25. Lakshmi, U.R.; Srivastava, V.C.; Mall, I.D.; Lataye, D.H. Rice husk ash as an effective adsorbent: Evaluation of adsorptive characteristics for Indigo Carmine dye. *J. Environ. Manag.* **2009**, *90*, 710–720. [CrossRef]

26. Riyap, H.I.; Bewa, C.N.; Banenzoué, C.; Tchakouté, H.K.; Rüscher, C.H.; Kamseu, E.; Bignozzi, M.C.; Leonelli, C. Microstructure and mechanical, physical and structural properties of sustainable lightweight metakaolin-based geopolymer cements and mortars employing rice husk. *J. Asian Ceram. Soc.* **2019**, *7*, 199–212. [CrossRef]

27. Alghamdi, A.A.; Al-Odayni, A.-B.; Saeed, W.S.; Al-Kahtani, A.; Alharthi, F.A.; Aouak, T. Efficient Adsorption of Lead (II) from Aqueous Phase Solutions Using Polypyrrole-Based Activated Carbon. *Materials* **2019**, *12*, 2020. [CrossRef] [PubMed]

28. Jeyakumar, R.P.S.; Chandrasekaran, V. Adsorption of lead (II) ions by activated carbons prepared from marine green algae: Equilibrium and kinetics studies. *Int. J. Ind. Chem.* **2014**, *5*, 10. [CrossRef]

29. Salihi, I.U.; Kutty, S.R.M.; Isa, M.H. Adsorption of Lead ions onto Activated Carbon derived from Sugarcane bagasse. *IOP Conf. Ser. Mater. Sci. Eng.* **2017**, *201*, 012034. [CrossRef]

30. Staroń, P.; Płecka, A.; Chwastowski, J. Lead Sorption by Chrysanthemum indicum: Equilibrium, Kinetic, and Desorption Studies. *Water Air Soil Pollut.* **2021**, *232*, 22. [CrossRef]

31. Qaiser, S.; Saleemi, A.R.; Umar, M. Biosorption of lead from aqueous solution by Ficus religiosa leaves: Batch and column study. *J. Hazard. Mater.* **2009**, *166*, 998–1005. [CrossRef] [PubMed]

32. Kul, A.R.; Caliskan, N. Equilibrium and Kinetic Studies of the Adsorption of Zn(II) Ions onto Natural and Activated Kaolinites. *Adsorpt. Sci. Technol.* **2009**, *27*, 85–105. [CrossRef]

33. Chwastowski, J.; Staroń, P. Influence of Saccharomyces cerevisiae yeast cells immobilized on Cocos nucifera fibers for the adsorption of Pb(II) ions. *Colloids Surf. A Physicochem. Eng. Asp.* **2022**, *632*, 127735. [CrossRef]

34. Sekar, M.; Sakthi, V.; Rengaraj, S. Kinetics and equilibrium adsorption study of lead(II) onto activated carbon prepared from coconut shell. *J. Colloid Interface Sci.* **2004**, *279*, 307–313. [CrossRef]

35. Ghahremani, D.; Mobasherpour, I.; Mirhosseini, S.A. Sorption thermodynamic and kinetic studies of Lead removal from aqueous solutions by nano Tricalcium phosphate. *Bull. Soc. R. Sci. Liege* **2017**, *86*, 96–112. [CrossRef]